

Diagnosing Ocean Stirring: Comparison of Relative Dispersion and Finite-Time Lyapunov Exponents

DARRYN W. WAUGH

Earth and Planetary Sciences, The Johns Hopkins University, Baltimore, Maryland

SHANE R. KEATING

Courant Institute of Mathematical Sciences, New York University, New York, New York

MEI-LIN CHEN

NOAA/National Oceanographic Data Center, Silver Spring, Maryland

(Manuscript received 20 November 2011, in final form 28 February 2012)

ABSTRACT

The relationship between two commonly used diagnostics of stirring in ocean and atmospheric flows, the finite-time Lyapunov exponents λ and relative dispersion R^2 , is examined for a simple uniform strain flow and ocean flow inferred from altimetry. Although both diagnostics are based on the separation of initially close particles, the two diagnostics measure different aspects of the flow and, in general, there is not a one-to-one relationship between the diagnostics. For a two-dimensional flow with time-independent uniform strain, there is a single time-independent λ , but there is a wide range of values of R^2 for individual particle pairs. However, it is shown that the upper and lower limits of R^2 for individual pairs, the mean value over a large ensemble of pairs, and the probability distribution function (PDF) of R^2 have simple relationships with λ . Furthermore, these analytical expressions provide a reasonable approximation for the R^2 - λ relationship in the surface ocean flow based on geostrophic velocities derived from satellite altimeter measurements. In particular, the bimodal distribution, upper and lower bounds, and mean values from the ocean flow are similar to the analytical expressions for a uniform strain flow. How well, as well as over what integration time scale, this holds depends on the spatial and temporal variations within the ocean region being considered.

1. Introduction

Understanding horizontal dispersal and stirring in the oceans is important for a wide range of problems, and a variety of diagnostics have been used to quantify these processes in oceanic (and other) flows. These include the mean-square separation (“relative dispersion”) of particles and finite-size Lyapunov exponents (FSLEs; e.g., Lacorata et al. 2001; Haza et al. 2008; LaCasce 2008), finite-time Lyapunov exponents (FTLEs; e.g., Abraham and Bowen 2002; Waugh et al. 2006; Beron-Vera et al. 2008; Waugh and Abraham 2008), and effective diffusivity (e.g., Marshall et al. 2006), which have all been calculated using velocities from numerical simulations

or derived from altimetry. Some of these diagnostics can also be applied to direct tracer observations. Relative dispersion and finite-size Lyapunov exponents can be calculated from the spreading of surface drifters or floats (see LaCasce 2008, and references therein), whereas finite-time Lyapunov exponents have been inferred from the elongation of a tracer patch following its release (e.g., Abraham et al. 2000; Coale et al. 2004; Law et al. 2006). Even though these diagnostics have been applied in numerous studies, there are still many uncertainties about dispersion and stirring in the surface ocean. Some of this is because the relationships between different diagnostics of stirring are not well known. This makes it difficult to compare and combine different studies, which typically use different diagnostics and consider different regions and time periods.

Two diagnostics that are often considered together are relative dispersion R^2 and FSLEs. The relative dispersion

Corresponding author address: Darryn W. Waugh, Earth and Planetary Sciences, The Johns Hopkins University, 3400 N. Charles St., Baltimore, MD 21218.
E-mail: waugh@jhu.edu

is calculated from the squared separation of particle pairs, whereas the FSLE is based on the time for particles pairs to increase their separation from δ to $\alpha\delta$ (where $\alpha > 1$). Dimensional analysis provides a simple relationship between the temporal dependence of the ensemble-mean relative dispersion $\langle R^2 \rangle$ and the spatial dependence of the FSLE λ_S , and these relationships have been used to identify different dispersion regimes within ocean flows (e.g., Lacorata et al. 2001; Haza et al. 2008; LaCasce 2008). These studies have generally shown exponential spreading for small times and spatial scales ($\lambda_S \sim \text{constant}$ and $\langle R^2 \rangle \sim \exp 2\lambda_S t$) and slower algebraic growth for larger times and spatial scales ($\lambda_S \sim \delta^{-\beta}$ and $\langle R^2 \rangle \sim t^{2/\beta}$, with β in the range of 1–2), although there is not universally consistent results.

The FTLE is also related to the rate of separation of initially close particles, has been applied in several different studies to velocities calculated from model simulations, and can be calculated from direct tracer observations. However, there has been less attention paid to the relationship between FTLEs and other the diagnostics. In this study, we examine the relationship between FTLEs and R^2 . We focus on the comparison with R^2 rather than FSLE because there are several different approaches to calculating the FSLE with no consensus on best approach and results can be sensitive to method used (e.g., LaCasce 2008; Lumpkin and Elipot 2010). Also, observational estimates of both the FTLE and R^2 are being made during the Diapycnal and Isopycnal Mixing Experiment in the Southern Ocean (DIMES) experiment (Gille et al. 2007). Although both the FTLE and R^2 depend on the spreading of particle pairs, an important difference is that the R^2 (and FSLE) depends on the mean of an ensemble of particle pairs, whereas the FTLE depends only on the maximum spreading rate (see further discussion below).

In the next section, we calculate analytic expressions for the FTLEs and relative dispersion in two-dimensional flow with uniform strain and show that, even in this extremely simple case, there is not a one-to-one relationship between the two diagnostics: in particular, there can be a wide range of values of R^2 for each value of λ . Nonetheless, the mean, the upper and lower limits, and the probability distribution function (PDF) of R^2 have simple relationships with λ . In section 3, we test whether the relationships between R^2 and λ for uniform strain hold for ocean currents derived from satellite altimetry and hence whether the uniform strain flow is a useful model of the local flow in the surface oceans. Concluding remarks are in section 4.

2. Local strain flow

a. Steady strain

Before considering FTLEs and relative dispersion in ocean flows, we illustrate their relationship in a simple two-dimensional flow with uniform, time-independent strain,

$$\mathbf{u} = (\gamma x, -\gamma y). \quad (1)$$

The trajectory of a particle initially at (x_0, y_0) is given by $x(t) = x_0 e^{\gamma t}$, $y(t) = y_0 e^{-\gamma t}$. The squared separation of two particles initially separated by a distance δ_0 is

$$\delta r^2(t) = \delta_0^2 \cos^2 \theta_0 e^{2\gamma t} + \delta_0^2 \sin^2 \theta_0 e^{-2\gamma t}, \quad (2)$$

where $\theta_0 = \tan^{-1}(\delta y_0 / \delta x_0)$ is the orientation relative to the x axis of the line connecting the particles' initial locations. Note that this expression does not depend on the position of the center of mass of the particles or on the presence of a background spatially uniform ("sweeping") flow. The maximum spreading of particles occurs if the particles are aligned with the x axis ($\delta y_0 = 0$), with $\delta r(t) = \delta_0 e^{\gamma t}$ (see triangles in Fig. 1). In contrast, if initially aligned with the y axis ($\delta x_0 = 0$), the separation decreases as $\delta r(t) = \delta_0 e^{-\gamma t}$ (diamonds in Fig. 1). For other orientations, the spreading rate varies between these two limits. Thus, an ensemble of particles initially arranged in a circle of radius δ_0 will be stretched into an ellipse, with major axis increasing as $\delta_0 e^{\gamma t}$ and minor axis decreasing as $\delta_0 e^{-\gamma t}$, as shown in Fig. 1. The figure shows the case of a circle centered at the origin, in which case the center of the particles remains at the origin. For a circle initially centered away from the origin the center of the particles moves with the flow, but the trajectories of the particles relative to the center is the same as in this example.

The FTLE at location \mathbf{x}_0 can be defined as

$$\lambda(\mathbf{x}_0, t) = \frac{1}{t} \log \frac{\delta r(t)}{\delta r(0)}, \quad (3)$$

where δr is the separation of a pair of particles that were initially close together and centered at \mathbf{x}_0 and the initial orientation of the particles is chosen so that λ is maximal. For the uniform strain flow, the maximum stretching rate of two particles occurs when the pair is aligned with the x axis: that is, $\delta r(t) = \delta_0 e^{\gamma t}$. Hence, in this flow there is a single, time-independent FTLE that equals the strain rate of the flow: that is, $\lambda = \gamma$.

In contrast, the normalized relative dispersion of a pair of particles,

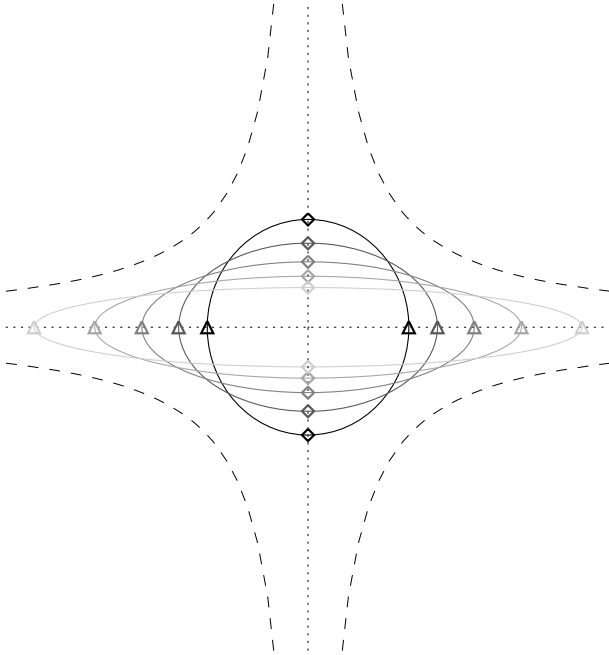


FIG. 1. Evolution of an initial circle in a strain flow. Curves show ellipse at $\gamma t = 0, 0.25, 0.5, 0.75,$ and 1 (e.g., days $0, 2.5, 5, 7.5,$ and 10 for $\gamma = 0.1 \text{ day}^{-1}$). Symbols show evolution of a pair of particles aligned with the expansion (triangles) or compression (diamond) axes of the strain, and black dashed curves show streamlines.

$$R^2(\mathbf{x}_0, t) = \delta r^2(t)/\delta r^2(0), \tag{4}$$

varies both with the initial alignment of the particles and with time. From (2), we see that the minimum and maximum values of R^2 are $e^{-2\gamma t}$ and $e^{2\gamma t}$, which correspond to the pairs being aligned with the x and y axis, respectively. As $\lambda = \gamma$ for this flow, it then follows that

$$R_\lambda^{-2} \leq R^2 \leq R_\lambda^2, \quad \text{with } R_\lambda = e^{\lambda t}. \tag{5}$$

This means that the upper and lower limits of the relative dispersion of individual pairs of particles can be calculated from λ . Alternatively, this can be expressed as

$$-\lambda \leq \lambda_R \leq \lambda, \quad \text{with } \lambda_R = \frac{1}{2t} \log(R^2). \tag{6}$$

The above considers the relative dispersion of individual particles. However, it is more common to consider the mean relative dispersion of an ensemble of N particles that have the same initial separation δ_0 but random orientations,

$$\langle R^2(t) \rangle = \frac{1}{N(N-1)} \sum_{i \neq j} R_{ij}^2(t), \tag{7}$$

where R_{ij}^2 is the relative dispersion of particles i and j (e.g., LaCasce 2008). Because the initial location of particles does not matter for relative dispersion in the uniform strain flow, this is equivalent to calculating the squared separation from the origin of an ensemble of particle initially evenly spread around a circle of radius δ_0 centered on the origin. Integrating (2) for the separation of each these particles from the origin and normalizing by δ_0^2 yields

$$\langle R^2 \rangle(t) = \frac{1}{2}(e^{2\gamma t} + e^{-2\gamma t}) = \frac{1}{2}(R_\lambda^2 + R_\lambda^{-2}) = \cosh(2\lambda t). \tag{8}$$

Figure 2 shows the temporal evolution of the $\langle R^2 \rangle$ together with that of minimum and maximum values of R^2 . Also shown (dotted-dashed lines) is $(1/2)R_\lambda^2$. This figure shows that the mean relative dispersion of an ensemble of particles is always less than R_λ^2 and that $\langle R^2 \rangle \approx (1/2)R_\lambda^2$ for $\gamma t > 1$. In other words, after a time scale of $1/\gamma$ the mean relative dispersion in uniform strain increases exponentially at a rate given by λ ($=\gamma$).

It is also possible to calculate the probability distribution function of R^2 for the ensemble of particles. If θ_0 is a random variable between $-\pi$ and π with uniform distribution $P(\theta_0) = 1/2\pi$, then we can make a change of variable from θ_0 to R^2 : that is, $P(R^2) = P(\theta_0)|d\theta_0/dR^2| = P(\theta_0)/[\sin 2\theta_0(R_\lambda^2 - R_\lambda^{-2})]$. Using (2) to eliminate θ_0 then yields

$$P(R^2) = \frac{1}{\pi \sqrt{(R^2 - R_\lambda^{-2})(R_\lambda^2 - R^2)}}. \tag{9}$$

This corresponds to an arcsine distribution, which is a special case of a beta distribution. Figure 3 shows $P(R^2)$ for $\gamma = 0.1 \text{ day}^{-1}$ and $t = 2.5, 5, 7.5,$ and 10 days (these are the same times shown in Fig. 1). The PDFs are bimodal, with peaks at the minimum and maximum values ($R^2 = R_\lambda^{-2}$ and R_λ^2). The breadth of the PDFs increases with time, with larger change in the upper limit than in the lower limit (as shown in Fig. 2). For increasing time the percentage of particle pairs with R^2 close to the mean value (dashed vertical lines in Fig. 3) decreases, and for $t = 10$ days there is only a very small percentage of particle pairs with $R^2 \approx \langle R^2 \rangle$.

The breadth of the PDFs and limited number of pairs with R^2 near the ensemble mean raises the question of how sensitive the ensemble-mean R^2 is to number of particle pairs. Monte Carlo simulations (not shown) indicate that greater than 100 pairs are needed to yield a robust estimate of the true $\langle R^2 \rangle$. For example, for 5

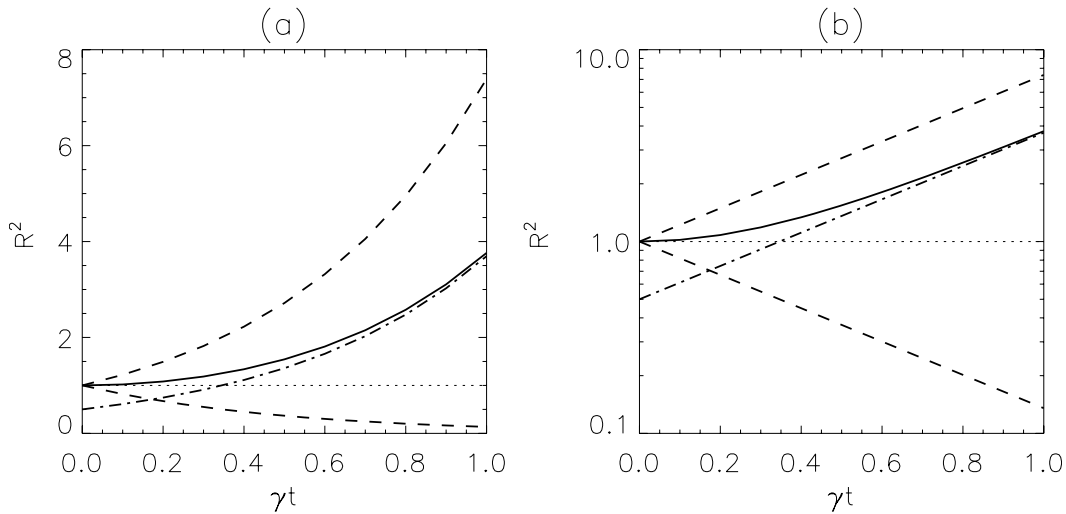


FIG. 2. Temporal evolution of mean (solid curves), minimum (lower dashed), and maximum (upper dashed) values of R^2 . Also shown (dotted-dashed lines) is $(1/2)R^2$. (a) A linear scale and (b) a logarithmic scale for R^2 .

pairs the probability that the mean of these pairs is within 10% of the true $\langle R^2 \rangle$ is only 20%, for 10 pairs the probability increases to 40%, but over 150 pairs are needed to have a 95% probability.

b. Time-varying strain

A more realistic model of a turbulent flow is the local gradient flow model,

$$\mathbf{u}(\mathbf{x}, t) = \mathbf{A}(t)\mathbf{x}, \tag{10}$$

where $\mathbf{A}(t)$ is the strain tensor. Here, $\mathbf{A}(t)$ can be decomposed into symmetric and antisymmetric parts,

$$\mathbf{S} = \begin{pmatrix} a(t) & b(t) \\ b(t) & -a(t) \end{pmatrix}, \quad \mathbf{\Omega} = \begin{pmatrix} 0 & \omega(t) \\ -\omega(t) & 0 \end{pmatrix}. \tag{11}$$

Incompressibility implies that \mathbf{S} is traceless with eigenvalues $\pm\gamma$, where $\gamma = \sqrt{a^2 + b^2} \neq 0$. It can be shown (e.g., Lapeyre 2002) that the normalized relative dispersion for this flow satisfies

$$\lambda_R(t) = \frac{1}{2t} \ln R^2 = \overline{\gamma \cos 2\phi}, \tag{12}$$

where ϕ is the orientation of a particle pair relative to the orientation of the strain axes and $\overline{} = t^{-1} \int_0^t () d\tau$ is

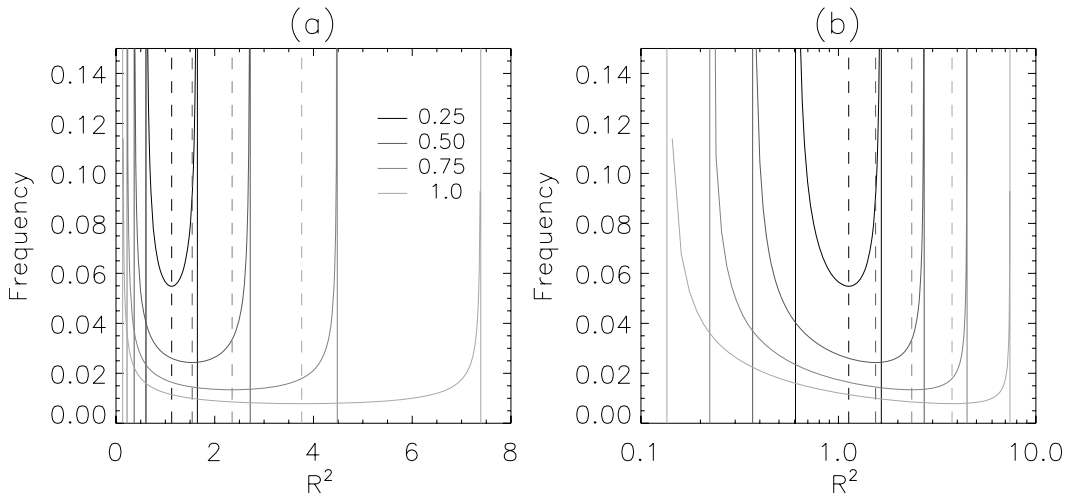


FIG. 3. PDFs of R^2 for $\gamma t = 0.25, 0.5, 0.75,$ and 1 (same values as in Fig. 1). Vertical dashed lines show mean R^2 . (a) A linear scale and (b) a logarithmic scale for R^2 .

a temporal average. Using the Cauchy–Schwarz inequality, we can bound this quantity from above,

$$|\lambda_R(t)| \leq |\bar{\gamma}| |\overline{\cos 2\phi}|. \quad (13)$$

Lapeyre (2002) demonstrates that particle pairs will align along the unstable Lyapunov direction ϕ_+ very quickly (exponentially fast in time), unless the pair is initially oriented along the stable Lyapunov direction. These latter pairs will make a negligible contribution to (13), so that we can assume that particle pairs are primarily distributed along ϕ_+ , and so

$$-\lambda(t) \leq \lambda_R(t) \leq \lambda(t), \quad \lambda(t) = \bar{\gamma} |\cos 2\phi_+|. \quad (14)$$

Thus, we recover the upper and lower bounds (6) and (7) with time-dependent Lyapunov exponent $\lambda(t)$. Note that both upper and lower bounds are sharp in the sense that there exist initial pair orientations that saturate the bounds: specifically, pairs orientated along the stable Lyapunov direction $\phi_- = \phi_+ \pm \pi/2$ will have $\lambda_R = -\lambda$, whereas all other pairs will ultimately saturate the upper bound $\lambda_R = \lambda$.

In the special case where the rotation of the flow equals the rotation of the axes (e.g., irrotational flow with stationary strain axes) the equations for the ensemble mean and PDF of R^2 are the same as for constant uniform strain [i.e., (8) and (9)]. In the more general case, this also holds for sufficiently short times, of order $t \approx |\gamma^2 - \omega^2|^{-1/2}$. After this time, the alignment process described above will increasingly weight the PDF toward the upper bound R_λ^2 . Thus, the ensemble average relative dispersion will grow as $\langle R^2 \rangle \approx R_\lambda^2$: that is, twice that in the case of the uniform strain flow.

3. Ocean flows

a. Data and methods

The flow considered in the previous section is very idealized, and we now consider more realistic ocean flows in which the strain varies with both space and time. We examine whether the relationships between R^2 and λ described above carry over and hence whether the uniform strain flow is a useful model of the local flow in the surface oceans.

Particle trajectories, and the above stirring diagnostics, are calculated using gridded absolute geostrophic surface velocities obtained from the Archiving, Validation, and Interpretation of Satellite Oceanographic data (AVISO). These geostrophic velocities are calculated from absolute sea level height that is the sum of merged altimeter measurements of anomalous sea

level and the mean dynamic topography of Rio and Hernandez (2004) and were used by Waugh and Abraham (2008) to examine the global variations in FTLEs. The gridded AVISO data are available on a $1/3^\circ$ Mercator grid every 7 days. However, it is important to note that the original gridded sea level anomalies are formed from the altimeter measurements using a mapping procedure with space and time correlation scales of around 150 km and 15 days, respectively (Ducet et al. 2000), so the effective resolution is lower than that of the gridded data. This means the velocities used in our calculations do not capture the stirring due to sub-mesoscale features (Poje et al. 2010; Keating et al. 2011). In the discussions below “ocean flow” refers to the flow resolved by the above geostrophic currents.

We calculate FTLEs as in Waugh et al. (2006) and Waugh and Abraham (2008). This does not involve tracking the actual separate of a pair of particles, but instead λ is calculated from the logarithm of the largest eigenvalue of $\mathbf{M}^T \mathbf{M}$, where \mathbf{M} is the integrated deformation obtained by integrating the Jacobian of the flow along a trajectory (for details, see Abraham and Bowen 2002). The trajectories are initialized on a regular 0.1° longitude by 0.1° latitude grid, covering the domain of interest.

To calculate the relative dispersion a second set of trajectories are calculated for particles on a second grid of the same size but displaced 1 km from the original grid. Combining the two sets of particles results in a grid of particle pairs that are 1 km apart that can be used to calculate the relative dispersion. Calculations have been repeated for grids displaced to the north, south, east, and west of the original grid and, although the values at specific locations depends on the orientation of the pair, the statistics over all pairs are the same in all cases.

We focus mainly on the flow within the Southern Ocean (50° – 65° S, 240° – 260° E) for December 2001–January 2002. (This is the general location of DIMES.) The robustness of the results obtained for this region is examined by repeating these calculations for several other regions of the ocean with differing mean strain.

b. R^2 – λ relationship

We first consider the spatial variations of λ and R^2 . Figure 4 shows maps of λ (Fig. 4a) and $\lambda_R = (1/2t) \log(R^2)$ (Fig. 4b) for 10-day integrations (we use λ_R rather than R^2 so it can be more easily compared with λ), plotted at the initial particle release locations. (The relative dispersion is calculated for particle pairs oriented east–west and 1 km apart; see above.) As shown in previous studies, there is wide range of values and finescale structure in the λ field, with low values inside coherent vortices and high values in filaments surrounding these vortices

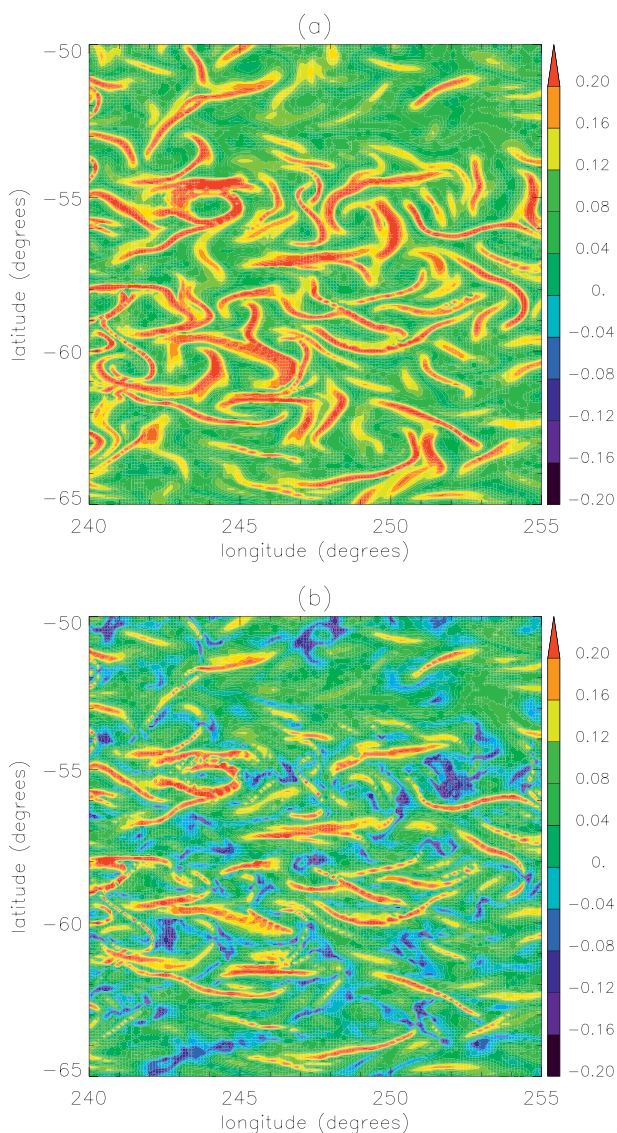


FIG. 4. Maps of (a) λ and (b) R^2 (expressed as λ_R to ease so compared with λ) for Southern Ocean region and integration time $t = 10$ days. Units are day^{-1} for both fields.

(e.g., Abraham and Bowen 2002; Waugh et al. 2006). The distribution of λ_R displays some similar features, with coherent regions of low values and filaments of high values. However, there are some significant differences: although λ is always positive, there are large regions with negative λ_R (which correspond to regions where particle pairs are converging), and there are many high- λ filaments where there are low values of λ_R . Thus, it is clear there is not a one-to-one relationship between the two fields.

To examine the R^2 - λ relationship in more detail, Fig. 5 shows scatterplots of R^2 versus λ for integration times $t = 5, 10, 15,$ and 20 days. Each point in the scatterplots

corresponds to particle initialized on the 0.1° by 0.1° grid, whereas the thick white curves show the mean R^2 for each value of λ . These plots clearly show that, for a given value of λ (and t), there is a large range of R^2 , including values greater than and smaller than unity (i.e., particles diverging and converging).

The analysis of uniform strain flow in the previous section can be used to help understand these variations. For given value of λ in the ocean flow, we can estimate the lower and upper limits and mean value of R^2 by assuming there is locally a uniform strain flow with $\gamma = \lambda$. This assumption is made only locally, and neighboring locations with different λ are assumed to have different local strain rates. The solid lines show the bounds on R^2 [(5)] and the dashed curves show the mean values [(8)], using this assumption. Overall, there is good agreement for the mean as well as lower and upper bounds of R^2 . The agreement starts breaking down for longer integration, and there is an increase in particle pairs where R^2 exceeds the upper limit and very few cases near the lower limit. These differences at long times are related to differences in the spatial scales over which the two diagnostics measure the stretching/dispersion. The FTLE measures the maximum integrated stretching in the vicinity of a single trajectory, whereas R^2 measures the spreading of actual pairs of particles and at long integration time a pair could be separated enough to be sampling different strain environments. These different environments could include regions with much larger strain and hence stretching than along the trajectory used for the FTLE calculation, which would result in individual values of R^2 exceeding the upper limit based on the λ . Smaller differences between λ_R and FTLE may occur if the FTLE was estimated from the actual separate of a pair of particles, rather than the method used here, which is not dependent in infinitesimal separations.

The similarities between the theoretical results for a uniform strain flow and the calculations using the ocean flow can also be seen by examining the PDFs of R^2 conditioned on the value of λ : that is, the conditional PDFs $P(R^2 | \lambda)$. Figure 6 compares $P(R^2 | \lambda)$ from the ocean flow with the analytical PDFs for uniform strain (Fig. 3), for $t = 10$ days and $\lambda = 0.025, 0.05, 0.075,$ and 0.1 day^{-1} . Even though the strain rate varies with space and time in the ocean flow, the PDFs for the ocean flow display many of the same characteristics of the PDFs for uniform strain flow. The $P(R^2 | \lambda)$ are generally bimodal with peaks near the upper and lower limits given by (5), the breath of the PDFs increase with integration time, and the percentage of pairs with R^2 near the mean value decreases with integration time. The peaks of the PDFs

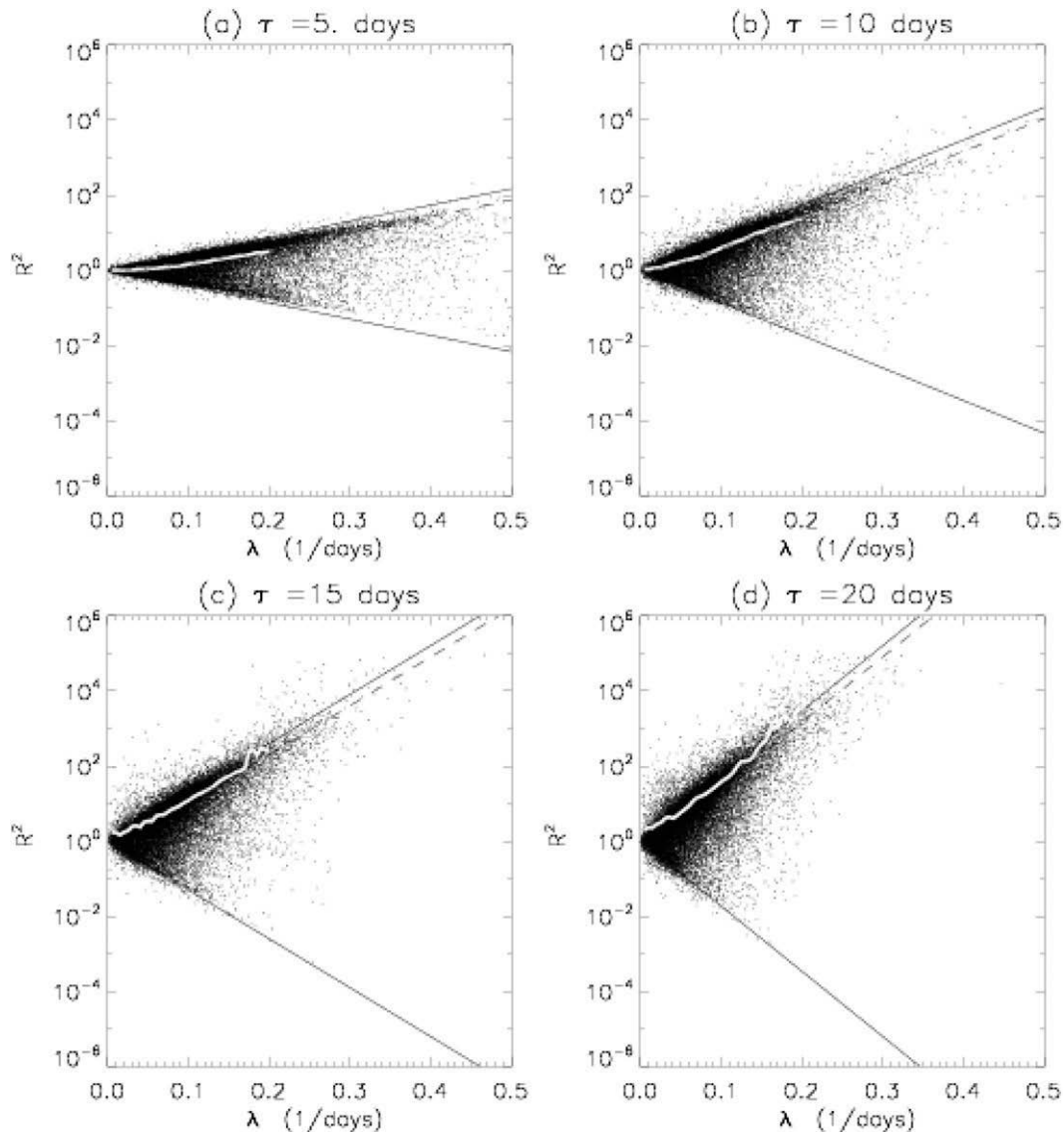


FIG. 5. Scatterplots of R^2 vs λ , for $\tau = 5, 10, 15,$ and 20 days. White curve is mean R^2 for given λ , and black curves show mean (dashed) and bounds (solid) of R^2 for uniform strain flow (with strain rate = λ).

in the ocean flow are broader than for uniform strain flow, and for large λ there is not a clear peak for large R^2 .

Trajectory and FTLE calculations similar to the above have been performed for other ocean regions. The results for all regions are qualitatively similar to that for the Southern Ocean region considered above. For example, Fig. 7 shows the R^2 - λ relationship for regions in the western North Atlantic Ocean (25° - 40° N, 290° - 305° E) and eastern North Atlantic Ocean (15° - 30° N, 320° - 335° E), for the same period as the Southern Ocean calculations. In all ocean regions, there is a wide range of values of R^2 for locations with the same λ , and the uniform strain flow provides reasonable approximation for mean and bounds for R^2 , at least for small integration

times. There are, however, quantitative differences between regions. In particular, there is a smaller range of λ and the uniform strain flow model fits for longer integration times in the eastern North Atlantic region than in the western North Atlantic or Southern Ocean regions. Similarly, the conditional PDFs $P(R^2|\lambda)$ are close to those for uniform strain flow for longer integration times in the eastern North Atlantic region.

These differences between regions are related to differences in the strain distribution within the regions. For spatially and temporally varying flows, the R^2 - λ relationship from uniform strain flow still provide a reasonable bound if the spatial variations of the strain are weak over the length scales of the particle separations. (The

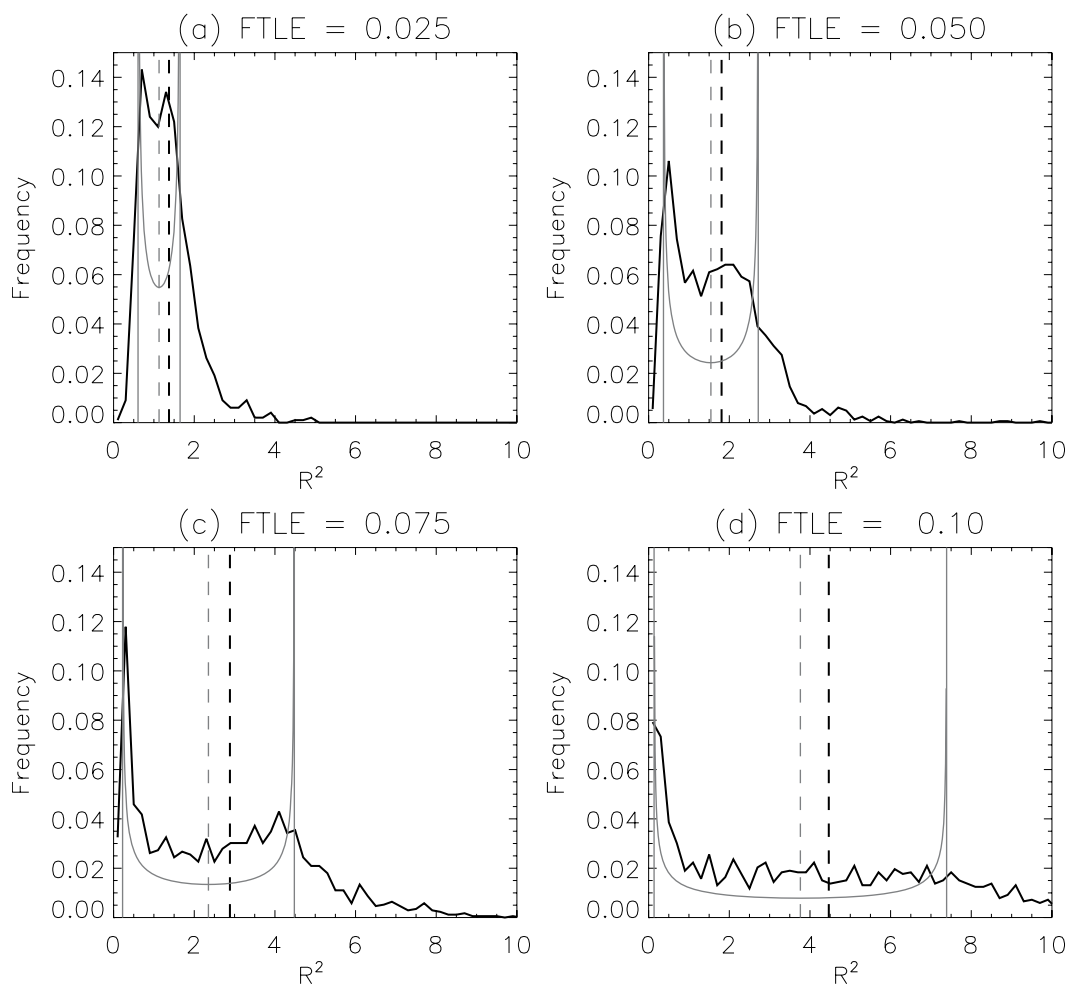


FIG. 6. Conditional PDFs of R^2 for 10-day integrations with λ equal to (a) 0.025, (b) 0.05, (c) 0.075, and (d) 0.1 day^{-1} , for Southern Ocean region (black curves) and a uniform straining flow (gray curves). Vertical dashed lines show mean R^2 .

relevant spatial variations are those in a Lagrangian framework following the particle trajectory.) We therefore would expect the bound to be better and to hold for longer integration times, in flows with more uniform strain rates. There are smaller values and less spatial variations of the strain rate within the eastern North Atlantic than the other regions considered, and this results in similar differences in λ (see Waugh and Abraham 2008). Consistent with the above expectations, the uniform strain bounds apply best and for longer in the eastern North Atlantic region. The difference in the R^2 - λ relationship between the Southern Ocean and western North Atlantic are also consistent with differences in distribution of strain rates between these two regions. See below for further discussion of differences between regions.

The comparisons above have considered the case where λ and R^2 are known for locations throughout

a domain. Although this is possible for model calculations, this is not a likely scenario for estimates from observations. Estimates of λ are only available from tracer releases at a few locations, and comparisons of λ with R^2 will only be meaningful if there has also been a release of multiple floats at the same location (as done in DIMES). We have performed such calculations using the altimeter-derived flow (i.e., simulated the evolution of a ring of particles a small distance from a central particle), and the resulting $P(R^2)$ are very similar to the conditional PDFs $P(R^2 | \lambda)$ calculated above if λ is that of the central location of the cluster (not shown). In particular, we also find for these calculations that consideration of a uniform shear flow with strain rate equal to the local λ provides a useful approximation of the distribution of R^2 for a cluster of particles released around the initial location of the λ calculation.

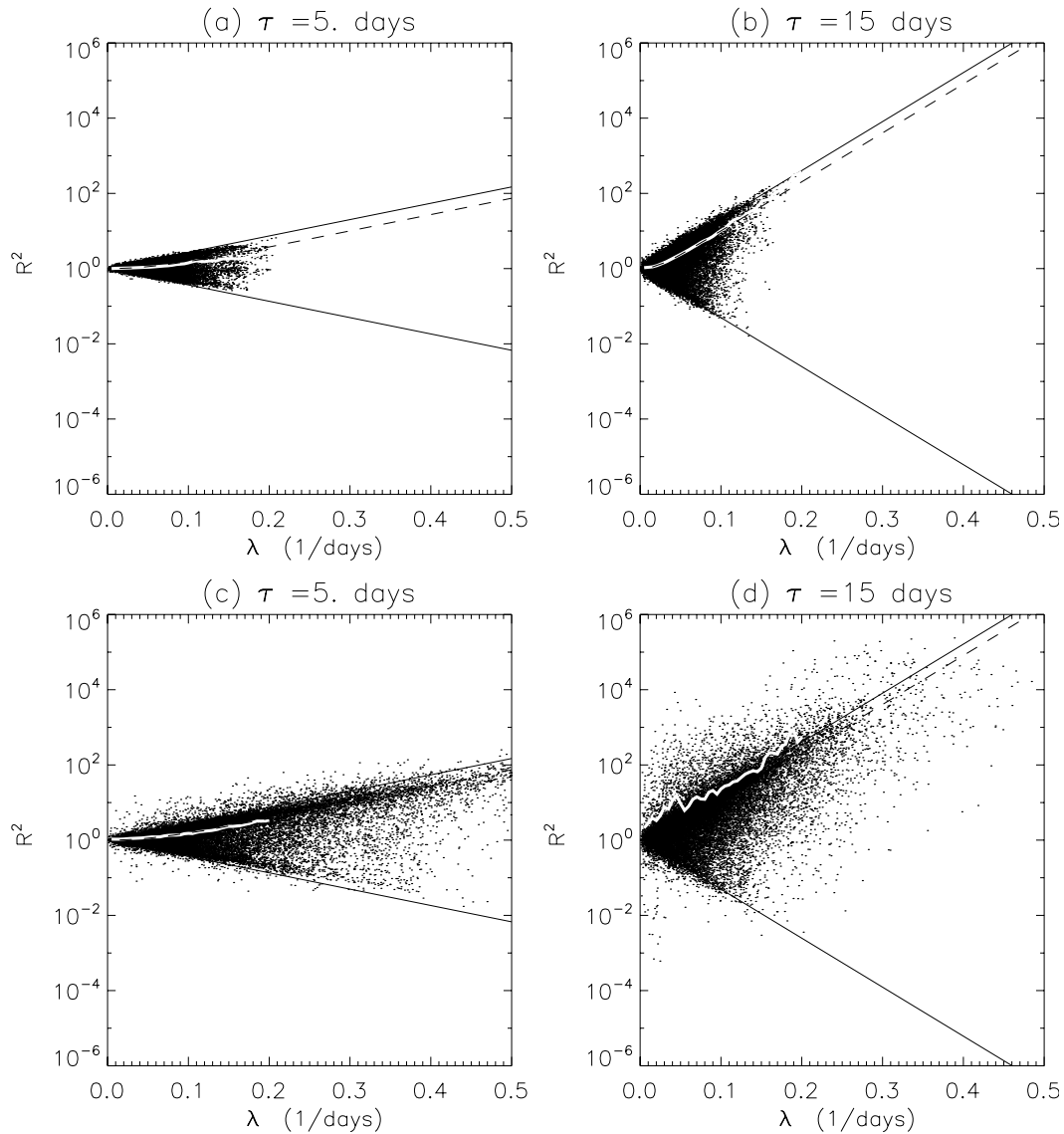


FIG. 7. As in Fig. 5, but for regions in the (a),(b) western and (c),(d) eastern North Atlantic Ocean, for τ equal to (a),(c) 5 and (b),(d) 20 days.

c. Regional distributions

In the above analysis, we have considered the distribution of R^2 for locations with the same λ ; however, a more usual situation is to consider the distribution for all points within a given region: that is, the calculation of $\langle R^2 \rangle$ is normally done for all particles or drifters within a given domain. We therefore consider the distribution of λ and R^2 for all locations within a given domain.

There is a wide range of λ within the domains considered here (see Fig. 5), and the $P(\lambda)$ are broad with a single peak at low values (e.g., Fig. 8a) (see also Waugh et al. 2006; Waugh and Abraham 2008). The broadness of $P(\lambda)$ is related to the nonuniformity of the strain rate

γ within the ocean flow, and for short integration times the PDF of λ is similar to the PDF of the strain rate γ (e.g., Waugh et al. 2006).

The PDFs of $P(R^2)$ for all locations within the Southern Ocean are also broad, with peaks at small R^2 (see Fig. 8b). These PDFs are very different from the conditional PDFs $P(R^2 | \lambda)$ shown above. The differences between the domain-wide $P(R^2)$ and the conditional $P(R^2 | \lambda)$ can be understood by using Bayes' theorem and writing the domain-wide PDF as

$$P(R^2) = \int \left(P(R^2 | \lambda) P(\lambda) \right) d\lambda. \quad (15)$$

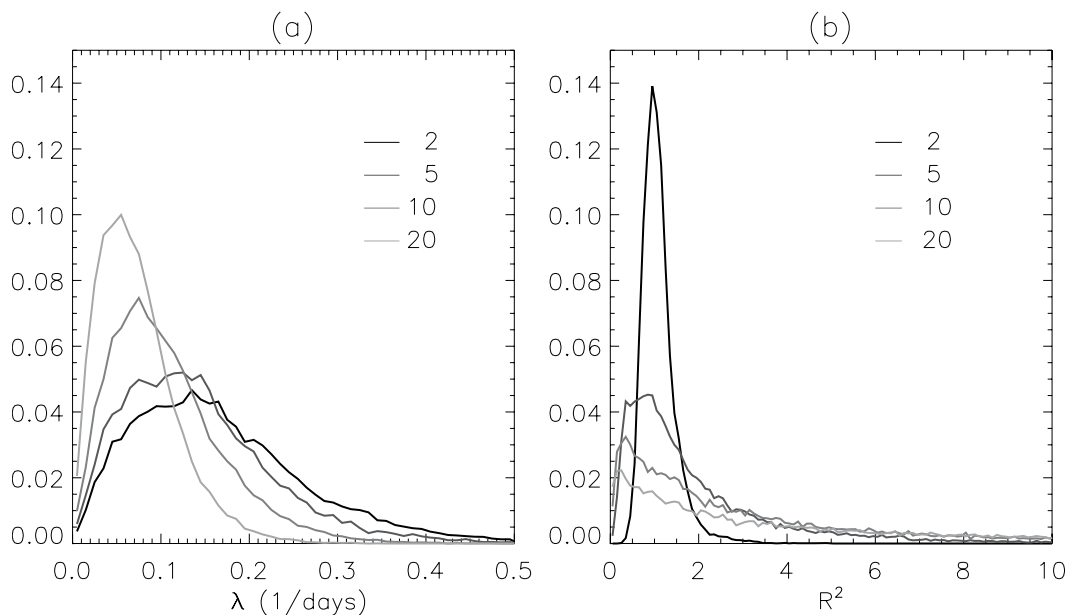


FIG. 8. PDFs of (a) FTLE and (b) $\log(R^2)$ for Southern Ocean region and integration time of 2, 5, 10, and 20 days. The darkest curves correspond to $t = 2$ days, and the lightest curves correspond to $t = 20$ days.

As shown above, the conditional PDFs $P(R^2 | \lambda)$ are bimodal with peaks near extreme values of R^2 , with the extrema in R^2 varying with λ (see Fig. 6). Further, the increase in maximum R^2 with λ is much larger than the decrease in the minimum R^2 . Combined together, the above means that the peaks at high R^2 are averaged out in the integration in (15) because the locations of peaks vary a lot with λ , whereas the peaks at low R^2 tend to superimpose. The result of the integration is then a broad, unimodal $P(R^2)$ with a peak at low R^2 .

An approximation of $P(R^2)$ can be formed using the simple uniform strain flow together with the result from previous studies that $P(\lambda)$ are well approximated by Weibull distributions (Waugh et al. 2006; Waugh and Abraham 2008),

$$P(\lambda) = \frac{b}{a} \frac{\lambda}{a}^{b-1} \exp\left(-\frac{\lambda^b}{a^b}\right). \quad (16)$$

Combining this with (9) as a model for $P(R^2 | \lambda)$ in (15) yields an estimate of $P(R^2)$.

Although the domain-wide PDFs of R^2 and λ are both broad and unimodal, the variation with integration time differs between the two diagnostics. Here, $P(\lambda)$ becomes narrower and the mean value $\langle \lambda \rangle$ decreases with integration time (e.g., Abraham and Bowen 2002; Waugh et al. 2006; Waugh and Abraham 2008), whereas $P(R^2)$ becomes broader and mean value $\langle R^2 \rangle$ increases with longer integration time. These differences are due to

the different quantities measured by the two diagnostics. The R^2 measures the separation of particles and, as shown in previous sections, for longer integration there is generally larger separation between particles. In contrast, λ measures the integrated strain along trajectories and, as particles remain in large strain regions only briefly, for longer integration times the particles spend more time in weak strain regions than regions with large strain and integrated strain decreases (Waugh et al. 2006).

The variation with integration time also differs between regions, with more rapid changes for regions with larger mean strain rates. This can be seen for the three regions considered above in Fig. 9. The spatial mean strain decreases from the western North Atlantic to the Southern Ocean and to eastern North Atlantic regions, and there is a similar variation in the mean λ shown in Fig. 9a (see also Waugh and Abraham 2008). For all regions, there is exponential growth of $\langle R^2 \rangle$ at early times and more algebraic growth at longer times (Fig. 9b). This is qualitatively similar to that found in previous ocean and atmospheric studies using ocean drifters or balloons (e.g., LaCasce 2008, and references therein). The transition from exponential to algebraic growth of R^2 occurs at earlier integration time for regions with larger strain rates; for example, the transition occurs at around 10 days for the western North Atlantic but after 25 days for the eastern North Atlantic regions.

The analysis above has focused on the distribution of R^2 . However, LaCasce (2010) recently examined the PDF and moments of the pair separation R , for

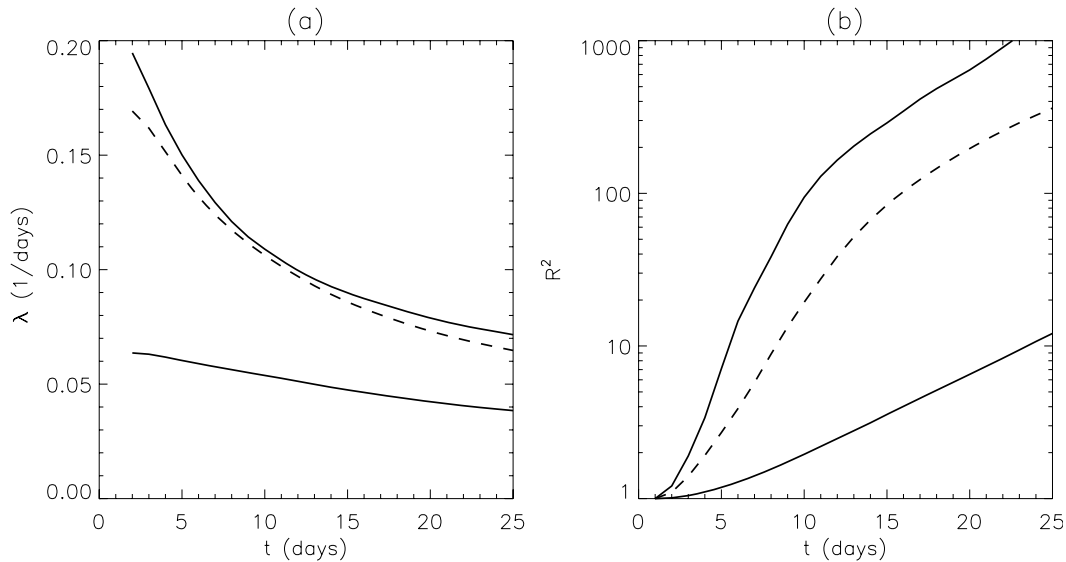


FIG. 9. Evolution of mean (a) FTLE and (b) R^2 with integration time, for Southern Ocean (dotted curves), western North Atlantic (solid), and eastern North Atlantic (dotted-dashed) regions.

several theoretical flows as well as ocean flows. He showed that within the enstrophy cascade range of two-dimensional turbulence (where the energy spectrum falls off as k^{-3}) the PDF of R is lognormal (see also Lundgren 1981; Bennett 2006) and that separation moments are given by $\langle R^n \rangle = R_0^n \exp[n(n+2)t/T_0]$ (where R_0 and T_0 are constants). For the above ocean flows, the separation moments are well fitted by these expressions, over the time where there is exponential growth in $\langle R^2 \rangle$ in Fig. 9b (i.e., 10–12 days in the western North Atlantic and Southern Ocean regions and over 25 days in the eastern North Atlantic region). This indicates that over these time periods the energy spectrum of the ocean flow falls off as (or faster than) k^{-3} .

The variation between regions in time for which the separation moments are well fit by analytical expressions for the enstrophy cascade range of two-dimensional turbulence is similar to variation in integration time for which the R^2 - λ relationship is well modeled by a uniform strain flow (see Figs. 5, 7).

4. Concluding remarks

The relationship between two commonly used diagnostics of stirring in ocean and atmospheric flows, the finite-time Lyapunov exponent λ and relative dispersion R^2 , is examined for a simple uniform strain flow and ocean flow inferred from altimetry. Both diagnostics are based on the spreading of particles. However, the two diagnostics measure different aspects of the flow,

and it is shown that in general there is not a one-to-one relationship between the diagnostics.

For the simple case of a two-dimensional flow with time-independent uniform strain, there is a single time-independent λ (which equals the strain rate), but there is a wide range of values of R^2 for individual particle pairs. This is because the FTLE is dependent on the maximum possible spreading rate, whereas relative dispersion is defined for any initial pair orientation. However, the distribution of R^2 , the upper and lower limits of R^2 for individual pairs, and the mean value over a large ensemble of pairs $\langle R^2 \rangle$ have simple relationships with λ . Specifically, the distribution of R^2 is an arcsine distribution that has peaks at upper and lower limits given by R_λ^2 and R_λ^{-2} , respectively, where $R_\lambda = e^{\lambda t}$. Thus, the particle pairs are separated into two populations corresponding to the expanding and contracting directions of the straining field. The ensemble average relative dispersion $\langle R^2 \rangle$ grows as $(1/2)R_\lambda^2$ on times long compared with the inverse strain rate; however, because of the bimodality of the arcsine distribution, there are relatively few particle pairs with this value of R^2 .

Temporal variability of the flow is straightforwardly incorporated into the uniform strain model by permitting the components of the strain tensor to change in time. In this case, the FTLE still provides an upper and lower bound on R^2 as before. These bounds are sharp in the sense that there exist initial pair orientations that saturate the bounds. When the strain axes are not constant in time, the distribution of R^2 is not evenly

distributed between expanding and contracting directions: as time increases, particle pairs align with the stretching direction and the PDF increasingly weights to the upper bound. Thus, on long times, $\langle R^2 \rangle$ grows at twice the rate of the steady case prediction. Even so, these observations suggest that certain elements of the simple, steady strain model might hold in more realistic turbulent flows.

In real-world ocean flows, the strain rate is spatially and temporally varying and there is a more complicated relationship between λ and R^2 . Nevertheless, the uniform strain flow still provides a useful approximation for the distribution, upper and lower bounds, and mean value of R^2 for locations in the ocean flow with the same λ , if the local λ is equated with the strain in the uniform-strain flow. How well this holds and over what integration time scale varies between regions and depends on the spatial and temporal variations within the region (in particular, the spatial variations of the strain over the length scales of the particle separations). For example, the uniform strain approximation holds for longer integration times in the quiescent eastern North Atlantic than in the more active western North Atlantic and Southern Ocean regions.

The relationships between λ and R^2 presented here could potentially be useful for the analysis and interpretation of observed diagnostics, for example, in comparing calculations of R^2 from drifters with estimates of λ from tracer release experiments. More generally, this analysis suggests that the uniform strain flow can be used as a useful conceptual model for understanding the dispersion and stirring in ocean flows. However, the limitations of the altimeter-derived flows are a potentially important restriction, and an outstanding issue is how well the uniform strain flow is a model for flows where submesoscale characteristics are resolved.

Indeed, it is possible that the limitations of the uniform strain model are being masked by the use of altimetric velocity fields, because the relatively low spatial resolution of the altimetry results in velocity fields that are smoother than they are in reality. However, in regions of the ocean where the eddy kinetic energy (EKE) spectrum falls off faster than k^{-3} for isotropic horizontal wavenumber k , it is actually the large-scale flow that governs the dispersion of particle pairs (Bennett 1984; Babiano et al. 1985). In these regions, R^2 and λ are relatively insensitive to the spatial resolution of the observations as long as the bulk of the inverse cascade range is resolved, which is generally the case for altimetric velocity fields (Keating et al. 2011). This stands in contrast to the classical Richardson (1926) scenario in which the dispersion of particle pairs is controlled by

eddies on the scale of the pair separation. Such a “spectrally local” picture of tracer mixing is appropriate for regions of the ocean with an EKE spectrum that falls off less sharply than k^{-3} , which is expected to occur when surface-trapped modes flatten the EKE spectrum at high wavenumbers (Klein et al. 2008). Understanding the mechanisms leading to such submesoscale energization, its geographical distribution, and its impact on stirring diagnostics such as Lyapunov exponents and relative dispersion are active areas of research (Keating et al. 2011; Tulloch et al. 2011).

Acknowledgments. This work is funded by the U.S. National Science Foundation. SRK is supported by National Science Foundation Grant OCE-0962054. We thank Joe LaCasce and Inga Koszalka for helpful discussions.

REFERENCES

- Abraham, E. R., and M. M. Bowen, 2002: Chaotic stirring by a mesoscale surface-ocean flow. *Chaos*, **12**, 373–381.
- , C. S. Law, P. W. Boyd, S. J. Lavender, M. T. Maldonado, and A. R. Bowie, 2000: Importance of stirring in the development of an iron-fertilized phytoplankton bloom. *Nature*, **407**, 727–730.
- Babiano, A., C. Basdevant, and R. Sadourny, 1985: Structure functions and dispersion laws for two-dimensional turbulence. *J. Atmos. Sci.*, **42**, 941–949.
- Bennett, A. F., 1984: Relative dispersion: Local and nonlocal dynamics. *J. Atmos. Sci.*, **41**, 1881–1886.
- , 2006: *Lagrangian Fluid Dynamics*. Cambridge University Press, 286 pp.
- Beron-Vera, F. J., M. J. Olascoaga, and G. J. Goni, 2008: Oceanic mesoscale eddies as revealed by Lagrangian coherent structures. *Geophys. Res. Lett.*, **35**, L12603, doi:10.1029/2008GL033957.
- Coale, K. H., and Coauthors, 2004: Southern Ocean iron enrichment experiment: Carbon cycling in high- and low-Si waters. *Science*, **304**, 408–414.
- Ducet, N., P. Y. Le Traon, and G. Reverdin, 2000: Global high-resolution mapping of ocean circulation from TOPEX/Poseidon and ERS-1 and-2. *J. Geophys. Res.*, **105**, 19 477–19 498.
- Gille, S. T., K. Speer, J. R. Ledwell, and A. C. Naveira Garabato, 2007: Mixing and stirring in the Southern Ocean. *Eos, Trans. Amer. Geophys. Union*, **88**, 382, doi:10.1029/2007EO390002.
- Haza, A. C., A. C. Poje, T. M. Özgökmen, and P. Martin, 2008: Relative dispersion from a high-resolution coastal model of the Adriatic Sea. *Ocean Modell.*, **22**, 48–65.
- Keating, S. R., K. S. Smith, and P. R. Kramer, 2011: Diagnosing lateral mixing in the upper ocean with virtual tracers: Spatial and temporal resolution dependence. *J. Phys. Oceanogr.*, **41**, 1512–1534.
- Klein, P., B. L. Hua, G. Lapeyre, X. Capet, S. Le Gentil, and H. Sasaki, 2008: Upper-ocean turbulence from high-resolution 3D simulations. *J. Phys. Oceanogr.*, **38**, 1748–1763.
- LaCasce, J. H., 2008: Statistics from Lagrangian observations. *Prog. Oceanogr.*, **77**, 1–29.
- , 2010: Relative displacement probability distribution functions from balloons and drifters. *J. Mar. Res.*, **68**, 433–457.

- Lacorata, G., E. Aurell, and A. Vulpiani, 2001: Drifter dispersion in the Adriatic Sea: Lagrangian data and chaotic model. *Ann. Geophys.*, **19**, 121–129.
- Lapeyre, G., 2002: Characterization of finite-time Lyapunov exponents and vectors in two-dimensional turbulence. *Chaos*, **12**, 688–698.
- Law, C. S., and Coauthors, 2006: Patch evolution and the biogeochemical impact of entrainment during an iron fertilisation experiment in the sub-Arctic Pacific. *Deep-Sea Res. II*, **53**, 2012–2033.
- Lumpkin, R., and S. Elipot, 2010: Surface drifter pair spreading in the North Atlantic. *J. Geophys. Res.*, **115**, C12017, doi:10.1029/2010JC006338.
- Lundgren, T. S., 1981: Turbulent pair dispersion and scalar diffusion. *J. Fluid Mech.*, **111**, 27–57.
- Marshall, J., E. Shuckburgh, H. Jones, and C. Hill, 2006: Estimates and implications of surface eddy diffusivity in the Southern Ocean derived from tracer transport. *J. Phys. Oceanogr.*, **36**, 1806–1821.
- Poje, A. C., A. C. Haza, T. M. Özgökmen, M. G. Magaldi, and Z. D. Garraffo, 2010: Resolution dependence of relative dispersion statistics in a hierarchy of ocean models. *Ocean Modell.*, **31**, 36–50.
- Richardson, L. F., 1926: Atmospheric diffusion shown on a distance-neighbour graph. *Proc. Roy. Soc. London*, **110A**, 709–737.
- Rio, M.-H., and F. Hernandez, 2004: A mean dynamic topography computed over the world ocean from altimetry, in situ measurements and a geoid model. *J. Geophys. Res.*, **109**, C12032, doi:10.1029/2003JC002226.
- Tulloch, R., J. Marshall, C. Hill, and K. S. Smith, 2011: Scales, growth rates, and spectral fluxes of baroclinic instability in the ocean. *J. Phys. Oceanogr.*, **41**, 1057–1076.
- Waugh, D. W., and E. R. Abraham, 2008: Stirring in the global surface ocean. *Geophys. Res. Lett.*, **35**, L20605, doi:10.1029/2008GL035526.
- , —, and M. M. Bowen, 2006: Spatial variations of stirring in the surface ocean: A case study of the Tasman Sea. *J. Phys. Oceanogr.*, **36**, 526–542.